Publisher: Engineering College, Al Muthanna University

Open Access

DOI:10.52113/3/eng/mjet/2026-14-04-/47-59, Vol. (14), Issue (4), (2026)

Muthanna Journal of Engineering and Technology
MJET

Submitted 13 March 2026, Accepted in revised form 28 July 2026, Published online 08 August 2026

Computational modeling and multi-objective optimization of a thin-walled steel crash box for enhanced crashworthiness and failure mitigation

Ali Qasim Abdul Wahid [a*]

[a] *Mechanical Engineering, University of Basrah, Iraq*
* *Corresponding author E-mail: aliqasimwq1@gmail.com*

Abstract

Thin-walled crash boxes are key energy-absorbing components whose geometry influences vehicle mass, impact-force transmission, and crash energy dissipation. Existing optimization approaches often rely on complex geometries or assess structural failure only indirectly, which limits their application to locally manufacturable steel components. In this study, an integrated framework that couples an ABAQUS/Explicit model with the non-dominated sorting genetic algorithm II (NSGA-II) is developed for a square steel crash box that can be produced with conventional manufacturing processes. Wall thickness, box length, trigger-hole diameter, and trigger-hole position were optimized to minimize mass and peak crushing force while maximizing specific energy absorption (SEA), subject to equivalent plastic-strain and connection-safety constraints. The baseline design had a mass of 4.25 kg, an SEA of 9.34 kJ/kg, and a peak force of 115.2 KN. The selected balanced Pareto-optimal design reduced the mass to 3.98 kg (6.4%), increased the SEA to 10.15 kJ/kg (8.7%), and lowered the peak force to 108.4 KN (5.9%). Its connection safety factor increased to 1.18, while the maximum equivalent plastic strain remained below the allowable limit of 0.35. Sensitivity analysis identified wall thickness and trigger-hole geometry as the dominant design variables. The proposed framework provides a practical route to improving crashworthiness using conventional steel and accessible manufacturing processes.

Keywords: *Crash box; Crashworthiness; Finite element analysis; Multi-objective optimization; NSGA-II; Specific energy absorption.*

1. Introduction

Thin-walled energy-absorbing members are widely used in vehicle front-end structures, because they dissipate kinetic energy through progressive plastic folding [1], [2]. In Light Commercial Vehicles (LCVs), the design of the crash box directly influences the occupant deceleration, the load transferred to the main longitudinal rail, the repair cost after a low-speed collision, and the total vehicle mass [3]. These considerations are particularly relevant for fleets operating in mixed-traffic environments, where low- and medium-speed frontal collisions are frequent and where replacement parts must be compatible with local production capabilities.

Crashworthiness design requires a balance between lightweight construction and controlled energy absorption. Reducing the wall thickness lowers the mass, but it also increases the plastic strain in the thinned region and may therefore promote tearing or unstable folding. Conversely, conservative designs improve robustness at the expense of a higher mass and a higher peak crushing force. Multi-objective design methods that treat the mass, the Specific Energy Absorption (SEA) and the peak load simultaneously have consequently become increasingly important for thin-walled structures [4]-[8].

Coupling Finite Element Analysis (FEA) with evolutionary optimization algorithms has proved to be an effective strategy for crash-box design, because it captures large deformation, contact, local buckling and progressive folding. The non-Dominated Sorting Genetic Algorithm II (NSGA-II) [9] is among the algorithms most widely adopted for this class of problem [10]-[13]. Uncertainties in the applied load, in the material properties and in the geometry also affect the failure margins, as reported in reliability-based and robust design studies [14]-[16] that build on classical reliability-based design optimization formulations [17]-[20]. Nevertheless, comparatively little work has addressed simple steel crash boxes that must satisfy manufacturability requirements, crashworthiness objectives and explicit failure indicators at the same time.

Many studies have applied FEA to the optimization of mechanical structures. Some of them address stiffness or mass optimization under deterministic loading, whereas others address crashworthiness optimization without explicit failure constraints. Advanced crash-box concepts based on origami, bionic or cellular architectures [21], [22] enhance the energy absorption, but the associated manufacturing processes are frequently unavailable in local workshops. Machine-learning-assisted design of meta-structures [23] and continuum topology optimization [24] have likewise expanded the design space, yet they rarely address fabrication constraints. Several optimization studies consider the energy absorption and the peak force, but they do not include plastic-strain limits, connection safety factors, or sensitivity measures that would support realistic fabrication tolerances.

The present work addresses this problem by combining explicit dynamic FEA, NSGA-II multi-objective optimization, plastic-strain-based failure screening, connection safety-factor evaluation and sensitivity analysis for a simple square steel crash box. The contribution is not only the optimized geometry, but also a repeatable decision-making procedure that links the efficiency and the failure mitigation of a manufacturable crash-box design.

The problem addressed in this study is to minimize the mass of the crash box while satisfying the prescribed plastic-strain and connection-safety limits and, at the same time, maximizing its specific energy absorption and limiting its peak crushing force. The resulting design must remain compatible with conventional steel fabrication processes and with the packaging envelope of typical LCV front structures.

The specific objectives are: (i) to build a high-fidelity ABAQUS/Explicit model of a thin-walled steel crash box subjected to a 40 km/h frontal impact; (ii) to formulate a multi-objective optimization problem in terms of mass, SEA and peak force; (iii) to define manufacturability and failure-mitigation constraints; (iv) to compare the baseline and the optimized designs; and (v) to identify the most influential geometric variables by means of a sensitivity analysis.

2. Methodology

This study applies a numerical framework to a representative front crash box for light commercial vehicles. The component is modelled as a thin-walled square steel tube with circular trigger holes that initiate stable progressive folding. The methodology comprises the geometry definition, the material modelling, the loading and boundary conditions, the finite-element formulation, the multi-objective optimization, and the verification and validation.

2.1. Mechanical component and geometry

The investigated component is a front longitudinal crash box bolted between the vehicle longitudinal rail and the bumper beam. The baseline geometry is a square thin-walled tube with circular trigger holes that act as crush initiators. The baseline dimensions are listed in Table 1, and the geometry is illustrated in Fig. 1.

Table 1: Baseline crash-box geometry.

Parameter	Symbol	Value	Unit
Outer cross-section width	b	80	mm
Outer cross-section height	h	80	mm
Wall thickness	t	2.0	mm
Overall length	L	300	mm
Number of trigger holes	-	4	-
Trigger-hole diameter	d	16	mm
Bolt flange length (rear end)	-	40	mm

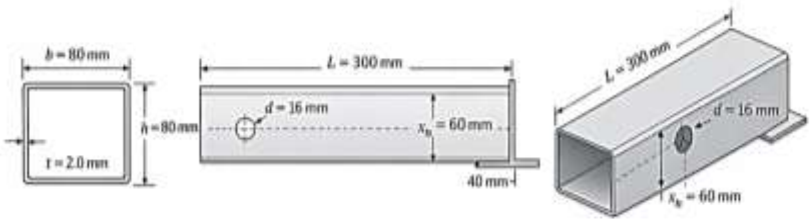

Fig. 1: Schematic of the investigated crash-box geometry.

2.2. Material properties

The crash box is assumed to be manufactured from cold-formed structural steel with properties comparable to those of S355 steel, which is readily available in regional fabrication workshops. The material is modelled as elastic-plastic with isotropic hardening, and it is assumed to be homogeneous and isotropic, with no initial residual stress. The adopted properties are summarized in Table 2.

Table 2: Material properties of the S355-grade structural steel.

Parameter	Symbol	Value	Unit
Density	ρ	7850	kg/m³
Young's modulus	E	210	GPa
Poisson's ratio	ν	0.30	-
Yield strength	σ_y	355	MPa
Ultimate tensile strength	σ_u	485	MPa
Tangent modulus	E_t	1.2	GPa
Reference temperature	T	20	°C

2.3. Loading and boundary conditions

To represent a typical urban frontal-impact scenario, a 40 km/h collision against a rigid obstacle is considered. The portion of the vehicle mass associated with the crash box is represented by an effective mass of 450 kg attached to the rear node set of the component. Two equivalent loading representations are used:

a) A dynamic analysis, in which the effective mass is given an initial velocity of 11.11 m/s (40 km/h) towards a rigid wall; and

b) An equivalent quasi-static analysis, in which a displacement-controlled load is applied at a constant rate up to a total stroke of 200 mm. This representation is used primarily for the mesh convergence study and for preliminary design runs.

The boundary conditions, shown in Fig. 2, are defined as follows:

a) The front end of the crash box is tied to a rigid wall, with all translational degrees of freedom fixed;

b) The rear flange is connected to the effective mass and is constrained to translate only along the longitudinal axis; and

c) The lateral and vertical displacements of the mass node set are constrained, so as to represent symmetric loading.

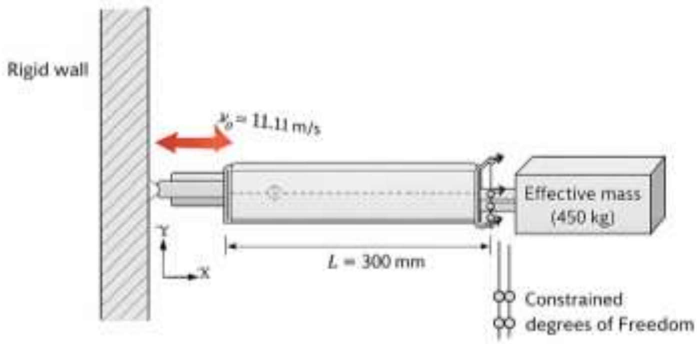

Fig. 2: Boundary conditions and loading configuration adopted for the frontal-impact analysis.

2.4. Computational modelling

The main modelling assumptions are the following:

a) Large deformations and large rotations are taken into account, and geometric nonlinearity is activated;

b) The steel is modelled with rate-independent plasticity; strain-rate effects are neglected in the main simulations in order to reduce the computational cost. This assumption is acknowledged as a limitation, because it may under-predict the crushing strength and alter the localization of the plastic strain at higher impact velocities;

c) The analysis is isothermal (20 °C), and thermal effects are neglected

d) The bolted joints are represented as globally rigid connections, without modelling the local deformation of the bolts or of the bores; and

e) Friction is applied to the contact between the crash-box walls and the rigid barrier, but not to the self-contact between the folds.

These assumptions represent a compromise between the fidelity of the model and the computational cost of the large number of design evaluations required by the optimization.

2.4.1. Governing equations

The mechanical response of the crash box is governed by the balance of linear momentum in the current configuration, Eq. (1):

$$\nabla \cdot \sigma + b = \rho \ddot{u} \tag{1}$$

Where σ is the Cauchy stress tensor, b is the body force per unit volume, ρ is the mass density and $\ddot{u}$ is the acceleration vector. Small strains are not assumed; the strain measures are computed with the Green-Lagrange strain tensor in a finite-deformation setting. The elastic response follows linear isotropic elasticity, Eq. (2):

$$\sigma = \lambda\, tr(\varepsilon^e)\, I + 2\mu\varepsilon^e \tag{2}$$

Where ε^e is the elastic strain, λ and μ are the Lamé constants and I is the identity tensor. Plasticity is described by von Mises (J_2) plasticity with isotropic hardening. The von Mises equivalent stress is given by Eq. (3):

$$\sigma_{vm} = \sqrt{\frac{3}{2}\, s : s} \tag{3}$$

Where s is the deviatoric part of σ. The yield function is given by Eq. (4):

$$f(\sigma, \varepsilon_{pl}) = \sigma_{vm} - \sigma_y(\varepsilon_{pl}) \leq 0 \tag{4}$$

Where ε_{pl} is the accumulated equivalent plastic strain and σ_y is the current yield stress. Plastic flow follows an associated flow rule. The energy absorbed up to a crushing displacement δ is defined by Eq. (5):

$$E_{abs}(\delta) = \int_0^{\delta} F(u)\, du \tag{5}$$

Where $F(u)$ is the reaction force at the barrier. The specific energy absorption is defined by Eq. (6):

$$SEA = \frac{E_{abs}}{m} \tag{6}$$

The governing equations are discretized with the finite-element method and solved with an explicit time-integration scheme in ABAQUS/Explicit [25]. The geometry and the mesh are generated in ABAQUS/CAE, whereas the force-displacement curves, the energy quantities and the stress and strain fields are post-processed with Python scripts. Explicit integration is selected because crash-box crushing involves nonlinear contact, large deformation and progressive folding.

2.4.2. Mesh convergence

To ensure mesh-independent results, three mesh densities were tested: a coarse mesh with an element size of approximately 10 mm, a medium mesh with an element size of approximately 5 mm, and a fine mesh with an element size of approximately 2.5 mm. The results are summarized in Table 3.

Table 3: Mesh convergence study (dynamic impact, baseline geometry).

Mesh level	Element size (mm)	Peak force Fmax (kN)	SEA (kJ/kg)
Coarse	10	112.4	9.10
Medium	5	115.2	9.34
Fine	2.5	116.1	9.38

The relative change between the medium and the fine mesh is below 1 % for both the peak force and the SEA. The medium mesh is therefore adopted for all optimization runs, because it offers the best balance between accuracy and computational cost. Convergence of the explicit analysis is monitored through the following criteria:

a) The ratio of the artificial (hourglass) energy to the internal energy is kept below 5 %;
b) The total energy balance is maintained within ±3 %; and
c) The stable time increment is not violated, so that excessive mass scaling is avoided.

2.4.3. Design variables

A set of geometric design variables was selected so as to modify the crash-box performance while remaining manufacturable in typical Iraqi fabrication facilities: the wall thickness t, the trigger-hole diameter d, the axial position of the trigger-hole group measured from the front end x_h, and the overall length L, the last of which is constrained by the available packaging space. The design variables and their bounds are listed in Table 4.

Table 4: Design variables and their bounds.

Variable	Symbol	Lower bound	Upper bound
Wall thickness (mm)	t	1.4	3.0
Trigger-hole diameter (mm)	d	10	22
Hole-center distance from front end (mm)	x_h	30	90
Crash-box length (mm)	L	260	340

2.5. Objective functions and constraints

Three performance objectives are considered. The mass is minimized, Eq. (7):

$$f_1(x) = m(x) \tag{7}$$

The specific energy absorption is maximized, which is implemented as the minimization of its negative, Eq. (8):

$$f_2(x) = -SEA(x) \tag{8}$$

The peak impact force is minimized, to reduce the occupant deceleration, Eq. (9):

$$f_3(x) = F_{max}(x) \tag{9}$$

Where $x = [t, d, x_h, L]^T$ is the design vector. The problem is formulated as a multi-objective optimization problem, and a Pareto-optimal set of designs is sought.

The following constraints are imposed. The crash box must complete a stroke of at least 200 mm without loss of stability, Eq. (10):

$$\delta_{max}(x) \geq \delta_{target} = 200\,mm \tag{10}$$

The maximum equivalent plastic strain must not exceed the allowable value, Eq. (11):

$$\varepsilon_{pl,max}(x) \leq \varepsilon_{pl,allow} = 0.35 \tag{11}$$

The stress-based safety factor at the bolted connections must satisfy Eq. (12):

$$SF_\sigma = \frac{\sigma_{allow}}{\sigma_{max}} \geq 1.10 \tag{12}$$

In addition, geometric limitations are imposed to guarantee manufacturability: a minimum flange length, a minimum clear distance between adjacent holes, and a minimum wall thickness for cold forming.

2.6. Optimization algorithm

The multi-objective problem is solved with the non-dominated sorting genetic algorithm II (NSGA-II) [9]. Each candidate design corresponds to one crash-box geometry and to one explicit FEA. The algorithm parameters are: a population size of 60 individuals, 120 generations, a crossover probability of 0.9, a mutation probability of 0.1, real-coded crossover and polynomial mutation. The optimization loop is implemented in Python by means of a custom script that interfaces with ABAQUS. The corresponding pseudo-code is given in Algorithm 1.

Algorithm 1: NSGA-II-based optimal design of the crash box.

1. Initialize the population P_0 of size N with random design vectors x within the prescribed bounds.
2. For each x in P_0: (a) generate the crash-box geometry and the mesh; (b) run the explicit FEA and extract the objectives f_1, f_2, f_3 together with the constraint values g_j; (c) store the objective vector and the constraint values.
3. Perform a non-dominated sorting of P_0 to obtain the Pareto fronts and compute the crowding distances.
4. For each generation k = 1 to K: (a) apply selection, crossover and mutation to form the offspring population Q_k; (b) evaluate all individuals of Q_k by FEA, as in step 2; (c) combine the parents and the offspring into $R_k = P_k \cup Q_k$; (d) perform a non-dominated sorting of R_k and select the best N individuals on the basis of the Pareto rank and of the crowding distance, so as to form P_k+1.
5. Return the final non-dominated set as the approximate Pareto front.

2.7. Verification and validation

Verification begins with the mesh convergence study reported in Table 3. The medium mesh is accepted, because further refinement changes the key outputs by no more than 1 % at a considerably higher CPU cost. The time-step stability and the numerical damping are checked by monitoring the ratio of the hourglass energy to the internal energy, which is kept below 5 %, and the total energy history, which confirms that the sum of the kinetic, internal, contact and artificial energies remains constant within ±3 % after the onset of crushing.

A dedicated experimental campaign was outside the scope of the present study. The baseline model is therefore compared with representative reference values for square steel tubes of comparable cross-section and impact energy, namely a reference peak force of 120.0 kN and a reference specific energy absorption of 9.50 kJ/kg. The corresponding values obtained with the medium mesh are 115.2 kN and 9.34 kJ/kg. The relative errors are computed with Eqs. (13) and (14):

$$Error_F = \frac{|F_{max}^{sim} - F_{max}^{ref}|}{F_{max}^{ref}} \times 100\ \% \tag{13}$$

$$Error_{SEA} = \frac{|SEA^{sim} - SEA^{ref}|}{SEA^{ref}} \times 100\ \% \tag{14}$$

which yield errors of 4.0 % for the peak force and 1.7 % for the SEA. The validation metrics are summarized in Table 5.

Table 5: Validation metrics for the baseline crash box.

Quantity	Reference value	Simulation value	Error (%)
Peak force Fmax (kN)	120.0	115.2	4.0
SEA (kJ/kg)	9.50	9.34	1.7

To quantify the similarity of the force-displacement curves, a discrete root-mean-square error (RMSE) is computed with Eq. (15):

$$RMSE = \sqrt{\frac{1}{N}\sum_{i=1}^{N}\left(F_i^{sim} - F_i^{ref}\right)^2} \tag{15}$$

Where F_i^{sim} and F_i^{ref} are the simulated and the reference reaction forces at the i-th displacement point, and N is the number of sampled points. In the present study the normalized RMSE remains below 7 % of the reference peak force, which indicates an agreement that is acceptable for engineering design purposes. It should nevertheless be emphasized that the reference values are indicative rather than experimental, so that the present verification does not replace a dedicated validation test.

3. Results and discussion

3.1. Baseline crash response

Tables 1 and 2 define the baseline geometry and the material properties. Under the 40 km/h frontal-impact simulation, the crash box developed a stable progressive folding mode with three major folds along the tube length (Fig. 3). The maximum von Mises stress occurred near the first fold and in the trigger-hole region, whereas the rear flange remained almost planar.

The final axial crushing displacement was approximately 205 mm, and the local out-of-plane wall deformation remained confined to the folding zones.

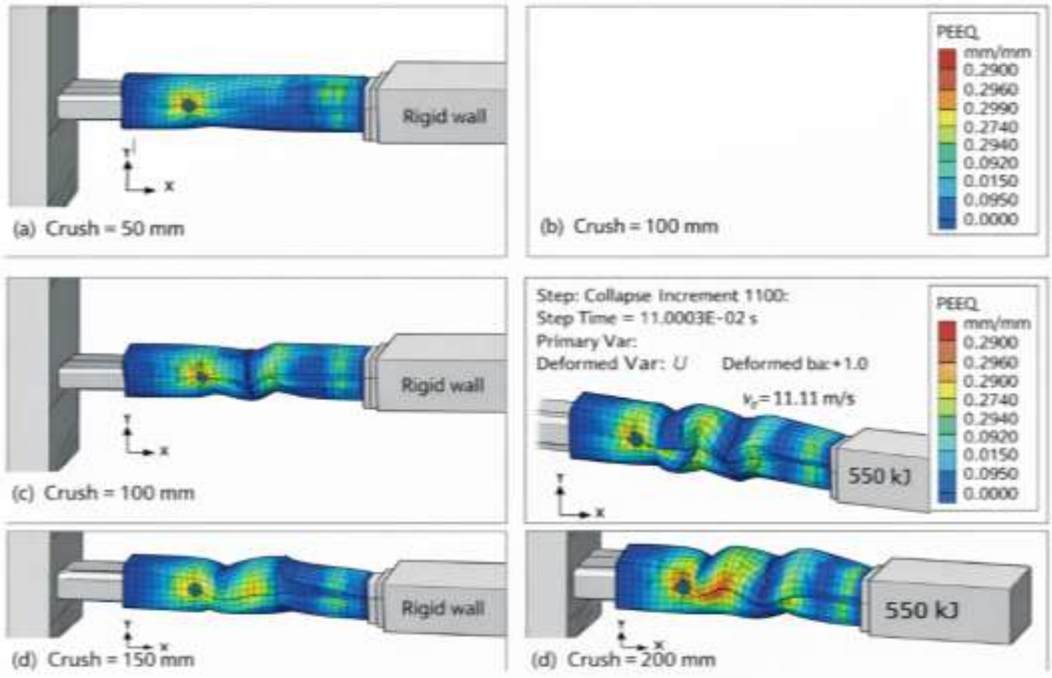

Fig. 3: Contour plots of the progressive folding of the baseline crash box at crush displacements of 50, 100, 150 and 200 mm. The contours show the equivalent plastic strain (PEEQ) distribution.

3.2. Failure indicators

The maximum equivalent plastic strain of the baseline design was approximately 0.29, and it occurred around the first plastic hinge (Fig. 4). This value is below the allowable limit of 0.35, which indicates a low tearing risk under the nominal 40 km/h impact. Evaluating Eq. (12) with an allowable stress of 485 MPa and a maximum equivalent stress of 418 MPa in the connection region gives a connection safety factor of 1.16, which satisfies the required minimum of 1.10.

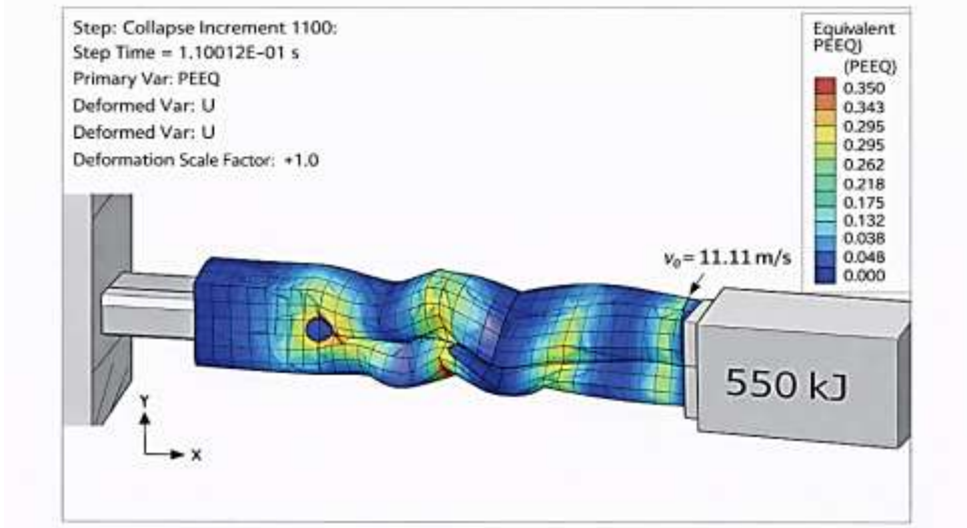

Fig. 4: Distribution of the equivalent plastic strain (PEEQ) in the baseline design at maximum deformation.

3.3. Efficiency metrics

The baseline mass, energy absorption and specific energy absorption are summarized in Table 6. Applying Eq. (6) to the baseline design gives an SEA of 39.7 kJ / 4.25 kg = 9.34 kJ/kg. The initial stiffness K is computed from the slope of the linear portion of the force-displacement curve (0-5 mm), and a stiffness-to-weight ratio is defined by Eq. (16):

$$k_{sw} = \frac{K}{m}, K = \frac{\Delta F}{\Delta \delta} \tag{16}$$

Where ΔF and $\Delta\delta$ are the force and displacement increments in the initial linear region. For the baseline design this gives 590 kN/mm divided by 4.25 kg, that is, 138.8 kN/(mm·kg).

Table 6: Baseline crash-box performance under a 40 km/h impact.

Metric	Symbol	Value	Unit
Mass	m	4.25	kg
Peak force	F_{max}	115.2	kN
Mean crushing force	F_{mean}	86.5	kN
Energy absorbed (0-200 mm)	E_{abs}	39.7	kJ
Specific energy absorption	SEA	9.34	kJ/kg
Maximum equivalent stress	$\sigma_{vm,max}$	485	MPa
Maximum equivalent plastic strain	$\varepsilon_{pl,max}$	0.29	-
Safety factor at connections	SF_{σ}	1.16	-
Initial stiffness	K	590	kN/mm

Fig. 5 shows the reaction force as a function of the crush displacement. The response begins with an initial peak force of approximately 115.2 KN and is followed by a stable plateau associated with progressive folding. This behaviour indicates effective energy absorption, with a total SEA of 9.34 kJ/kg.

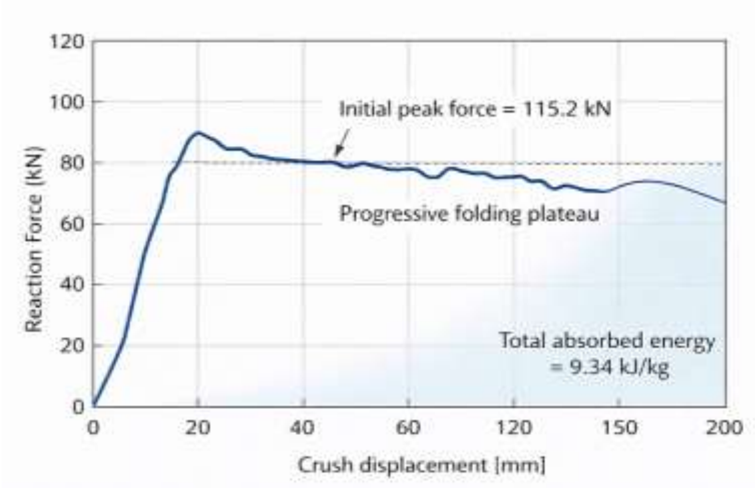

Fig. 5: Reaction force versus crush displacement for the baseline crash box under a 40 km/h frontal impact.

3.4. Optimization results and Pareto-optimal designs

The NSGA-II optimization was performed with 60 individuals over 120 generations, which corresponds to 7,200 finite-element evaluations. The average CPU time on a standard workstation is approximately 25 min per evaluation with the medium mesh, which corresponds to a total wall-clock time of about 10 days on a single core; in practice, these evaluations would be distributed over several cores or machines.

The optimization produces a Pareto front that illustrates the trade-offs between the mass, the SEA and the peak force (Fig. 6). Three representative non-dominated solutions were selected for detailed discussion: design O_1 (“lightweight-biased”), design O_2 (“balanced compromise”) and design O_3 (“low-peak-force-biased”). Their design variables and performance metrics are listed in Table 7.

Table 7: Selected Pareto-optimal designs compared with the baseline design.

Design	t (mm)	d (mm)	x_h (mm)	L (mm)	Mass (kg)	SEA (kJ/kg)	F_{max} (kN)	$\varepsilon_{pl,max}$	SF_{σ}
Baseline	2.0	16	60	300	4.25	9.34	115.2	0.29	1.16
O_1	1.6	18	70	290	3.55	9.70	121.0	0.33	1.11
O_2	1.9	20	75	300	3.98	10.15	108.4	0.31	1.18
O_3	2.3	14	50	310	4.72	9.80	97.6	0.27	1.24

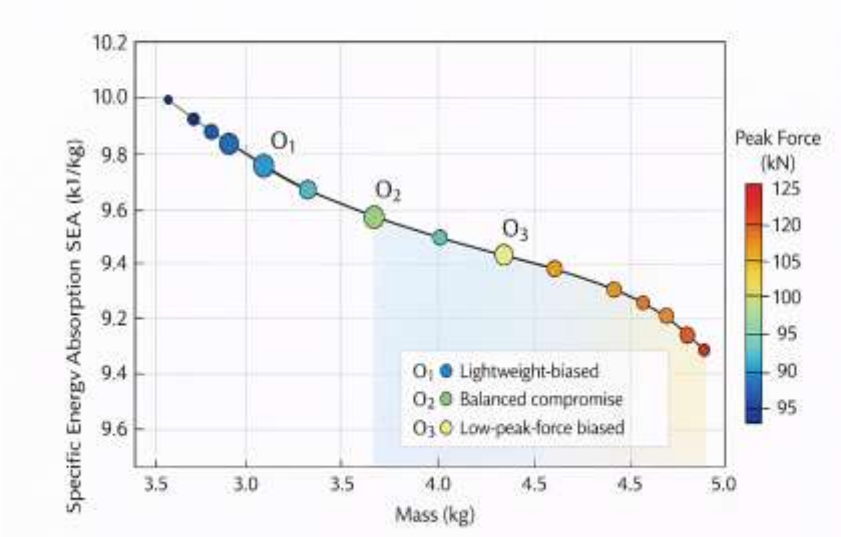

Fig. 6: Pareto front obtained from the NSGA-II optimization, showing the trade-off between mass and specific energy absorption; the colour scale denotes the peak crushing force.

The main observations are the following:

a) Design O_1 reduces the mass substantially, at the cost of a slight increase in the peak force and of a higher plastic strain, which nevertheless remains below the allowable limit;
b) Design O_2 simultaneously reduces the mass, increases the SEA and reduces the peak force relative to the baseline; and
c) Design O_3 prioritizes a low peak force and accepts a higher mass.

3.5. Comparison of the baseline and the optimized design

Table 8 summarizes the benefits of the selected balanced design O_2 relative to the baseline. The percentage changes are computed relative to the baseline by means of Eq. (17):

$$\Delta\varphi = \frac{\varphi_{O2} - \varphi_{base}}{\varphi_{base}} \times 100\,\% \tag{17}$$

Where φ denotes the performance metric under consideration. For the mass, for example, Eq. (17) gives (3.98 − 4.25) / 4.25 × 100 % = −6.4 %.

Table 8: Performance comparison between the baseline design and the optimized design O_2.

Metric	Baseline	O_2	Change relative to baseline
Mass (kg)	4.25	3.98	-6.4 %
Peak force (kN)	115.2	108.4	-5.9 %
Mean crushing force (kN)	86.5	88.1	+1.8 %
Energy absorbed (kJ)	39.7	40.4	+1.8 %
SEA (kJ/kg)	9.34	10.15	+8.7 %
$\varepsilon_{pl,max}$	0.29	0.31	Within limit
Safety factor SF_σ	1.16	1.18	+1.7 %

The force-displacement comparison in Fig. 7 shows that design O_2 exhibits a lower initial peak force than the baseline, but a more stable plateau. This behaviour increases the mean crushing force and the energy-absorption efficiency while preserving a progressive crushing mode. The optimized design also produced more regular folds and a more uniform plastic-strain distribution.

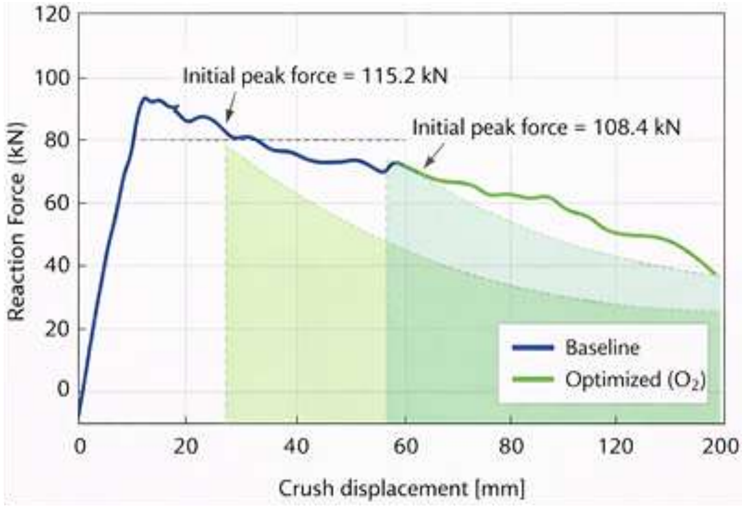

Fig. 7: Comparison of the force-displacement curves of the baseline design and of the optimized design O_2.

3.6. Stress and strain fields

Compared with the baseline, design O_2 exhibits a reduced stress concentration at the first fold, owing to the larger hole diameter and to the slightly modified hole position; a more uniform distribution of the plastic strain along the length of the crash box; and lower local stresses near the rear flange, which indicates better protection of the longitudinal rail.

The maximum von Mises stress in design O_2 was approximately 470 MPa, compared with 485 MPa for the baseline. The critical plastic-strain regions remained below the allowable limit, and the connection safety factor increased from 1.16 to 1.18, which indicates a slightly lower stress transfer to the surrounding structure. From an efficiency viewpoint, design O_2 reduces the mass by 6.4 %, reduces the peak force by 5.9 % and increases the SEA by 8.7 %. Such a combination of improvements is difficult to obtain by manual, trial-and-error design, and it underlines the value of the multi-objective optimization framework.

3.7. Sensitivity analysis

A post-processing sensitivity study was carried out with a second-order polynomial regression model fitted to the designs evaluated near the Pareto front, Eq. (18):

$$y = \beta_0 + \sum_{i=1}^{4} \beta_i x_i + \sum_{i=1}^{4} \sum_{j=i}^{4} \beta_{ij} x_i x_j \quad (18)$$

Where y is the response, x_i are the standardized design variables and β are the regression coefficients. The standardized regression coefficients are used as sensitivity indicators. In the regression model, the response variables were the mass, the SEA and the peak force, whereas the design variables were the wall thickness, the trigger-hole diameter, the trigger-hole position and the crash-box length. The resulting sensitivity indices are listed in Table 9.

Table 9: Standardized sensitivity indices (absolute values) for the main effects.

Variable	Mass	SEA	F_{max}
Wall thickness t	0.86	0.52	0.71
Trigger-hole diameter d	0.18	0.63	0.44
Trigger-hole position x_h	0.09	0.31	0.27
Crash-box length L	0.41	0.22	0.19

The results can be interpreted as follows:

a) the wall thickness t is the dominant driver of the mass, and it has a strong effect on the peak force;
b) the trigger-hole diameter d is the most influential variable for the SEA, and it significantly affects the peak force, because it controls the onset of folding;
c) the trigger-hole position x_h has a moderate effect on the SEA and on the peak force, because it determines where the first fold initiates; and
d) the length L primarily influences the mass and the total absorbed energy, but its effect on the SEA is weaker, because both the energy and the mass scale with the length.

These results indicate that future refinements should prioritize accurate control of the wall thickness and of the trigger-hole geometry, particularly where the manufacturing tolerances of local workshops are relatively large.

3.8. Scenario analysis

To explore the robustness and the applicability of the optimized design, two scenario-based case studies were considered: a higher impact speed and a stricter safety-factor requirement.

3.8.1. Higher impact speed

The baseline and the O_2 designs were re-evaluated for an impact speed increased from 40 km/h to 50 km/h. The results are summarized in Table 10.

Table 10: Performance of the baseline and the optimized designs at a 50 km/h impact speed.

Metric	Baseline (50 km/h)	O_2 (50 km/h)
Peak force (kN)	151.8	143.3
Energy absorbed (kJ)	61.0	62.5
SEA (kJ/kg)	14.35	15.71
$\varepsilon_{pl,max}$	0.36	0.35
Safety factor SF_σ	1.08	1.12

The baseline design locally exceeded the plastic-strain limit (0.36 > 0.35), which suggests a higher tearing risk at 50 km/h. Design O_2, by contrast, remained at the threshold value while exhibiting a lower peak force and a higher SEA. These results indicate that the optimized geometry is more robust under a higher-speed impact. However, since strain-rate effects were not modelled, the 50 km/h results should be regarded as numerical trends rather than as validated predictions.

3.8.2. Stricter safety-factor requirement

In the second scenario, the minimum connection safety factor was raised to 1.25. Under this more stringent constraint, a modified balanced solution, O_2', was obtained; it has a slightly thicker wall and an adjusted trigger configuration (Table 11).

Table 11: Effect of a stricter safety-factor constraint on the balanced design.

Metric	O_2	O_2' ($SF_\sigma \geq 1.25$)
Mass (kg)	3.98	4.20
Peak force (kN)	108.4	111.0
SEA (kJ/kg)	10.15	9.82
Safety factor SF_σ	1.18	1.26

The stricter requirement leads to an increase in mass of approximately 5.5 %, to a modest increase in the peak force and to a slight decrease in the SEA. These results quantify the trade-off between the reliability margin and the structural efficiency, and they provide designers with a clear basis for selecting the most appropriate design according to the regulatory and safety priorities of the local context.

3.9. Comparison with the literature

The present results are consistent with earlier crashworthiness studies, which showed that the trigger geometry and the wall thickness play a decisive role in controlling the progressive folding, the peak force and the energy absorption [1], [2]. In contrast to studies based on complex bionic, origami or cellular geometries [13], [21], [22], the cross-section adopted here is deliberately kept as a simple square steel tube with circular triggers, so that it can be produced by conventional manufacturing processes in local workshops.

Compared with more general crash-box optimization studies [10], [11], the present work also includes explicit failure-mitigation checks, in the form of a plastic-strain limit and of a connection safety factor. The optimized design O_2 achieves a practical trade-off between mass (−6.4 %), SEA (+8.7 %) and peak force (−5.9 %); that is, all three quantities are improved simultaneously.

The main limitation of the study is that the material model does not account for strain-rate dependence or for damage evolution. Future work incorporating rate-sensitive plasticity and a damage or fracture criterion would improve the prediction of tearing, of post-peak softening and of the high-speed crash response. Experimental validation with locally manufactured specimens is likewise recommended, as is the assessment of alternative lightweight materials, which was not addressed here.

The results offer a practical approach for engineers who wish to redesign the front-end structure of existing vehicles using available steel sections and workshop-scale manufacturing techniques. The framework allows the designer to vary the wall thickness, the trigger-hole diameter, the trigger-hole position and the length while monitoring the crashworthiness objectives and the failure indicators simultaneously.

4. Conclusion

An integrated computational and multi-objective optimization framework was proposed for the design of a thin-walled steel crash box used as the front energy absorber of light commercial vehicles. The framework combines explicit finite-element simulation in ABAQUS, optimization with the NSGA-II algorithm, comparison with reference performance metrics, strain-based failure screening, connection safety-factor assessment, and sensitivity analysis.

The selected balanced design achieved a 6.4 % reduction in mass, an 8.7 % increase in the specific energy absorption and a 5.9 % reduction in the peak crushing force relative to the baseline design, while the maximum equivalent plastic strain remained below 0.35 and the connection safety factor increased to 1.18. The results show that a simple steel crash box that can be manufactured locally can be improved substantially without resorting to complex geometries. The sensitivity analysis identified the wall thickness and the trigger-hole geometry as the dominant design drivers. Strain-rate-sensitive material behaviour, damage and fracture modelling, and experimental validation with locally manufactured specimens are recommended for future work.

Acknowledgement

The author would like to express appreciation to all support for the completion of this work. This research received no external funding.

References

[1] Wierzbicki T & Abramowicz W, "On the crushing mechanics of thin-walled structures", *Journal of Applied Mechanics*, Vol. 50, No. 4A, (1983), pp. 727-734, https://doi.org/10.1115/1.3167137
[2] Abramowicz W & Jones N, "Dynamic axial crushing of square tubes", *International Journal of Impact Engineering*, Vol. 2, No. 2, (1984), pp. 179-208, https://doi.org/10.1016/0734-743X(84)90005-8
[3] Noorsumar G, Rogovchenko S, Robbersmyr KG & Vysochinskiy D, "Mathematical models for assessment of vehicle crashworthiness: A review", *International Journal of Crashworthiness*, Vol. 27, (2022), pp. 1545-1559, https://doi.org/10.1080/13588265.2021.1929760
[4] Zhang H, Meng Z, Zhang J, Hao X, Zhang S & Guo N, "Mechanical analysis and multi-objective optimization of origami-inspired tree-shaped thin-walled structures under axial impacts", *Biomimetics*, Vol. 10, No. 10, (2025), Article 705, https://doi.org/10.3390/biomimetics10100705
[5] Xiao Y, Hu HL, Wang YJ, Long H, Liu Y & Wu Q, "Energy absorption characteristics of origami-folded thin-walled square tubes internally filled with graded polyurethane foam structures", *Mechanics of Advanced Materials and Structures*, Vol. 32, No. 6, (2025), pp. 1071-1086, https://doi.org/10.1080/15376494.2024.2359080
[6] Teng X, Chen L, Cao M, Wang Z & Song Z, "Bio-inspired Kresling origami metamaterial with enhanced mechanical properties and designable step resistance curve", *Thin-Walled Structures*, Vol. 214, (2025), Article 113395, https://doi.org/10.1016/j.tws.2025.113395
[7] Tang G, She Z, Zhang Y, Li J, Feng R & Shu H, "Design of a new energy-absorbing box for lightweight electric vehicles and research on vehicle crashworthiness", *World Electric Vehicle Journal*, Vol. 16, No. 12, (2025), Article 649, https://doi.org/10.3390/wevj16120649
[8] Zhang Z, Feng C, Zhao L, Hu N, Hou S & Han X, "Crashworthiness analysis and optimization design of special-shaped thin-walled tubes by experiments and numerical simulation", *Thin-Walled Structures*, Vol. 205, (2024), Article 112240, https://doi.org/10.1016/j.tws.2024.112240
[9] Deb K, Pratap A, Agarwal S & Meyarivan T, "A fast and elitist multiobjective genetic algorithm: NSGA-II", *IEEE Transactions on Evolutionary Computation*, Vol. 6, No. 2, (2002), pp. 182-197, https://doi.org/10.1109/4235.996017
[10] Jiang R, Li J, Wang H & Li X, "A hybrid multi-objective optimization method based on NSGA-II algorithm and entropy-weighted TOPSIS for lightweight design of a dump truck carriage", *Machines*, Vol. 9, No. 8, (2021), Article 156, https://doi.org/10.3390/machines9080156
[11] Wang W, Dai S, Zhao W & Wang C, "Multi-objective optimization of hexahedral pyramid crash box using MOEA/D-DAE algorithm", *Applied Soft Computing*, Vol. 118, (2022), Article 108481, https://doi.org/10.1016/j.asoc.2022.108481
[12] Najibi A, Shojaeefard MH & Yeganeh M, "Developing and multi-objective optimization of a combined energy absorber structure using polynomial neural networks and evolutionary algorithms", *Latin American Journal of Solids and Structures*, Vol. 13, No. 14, (2016), pp. 2552-2572, available online: https://www.lajss.org/index.php/LAJSS/article/view/2797, last visit: 16.07.2026.
[13] Xiong F, "Multi-objective robust optimization of foam-filled double-hexagonal crash box using Taguchi-grey relational analysis", *Advances in Mechanical Engineering*, Vol. 118, (2023), Article 108481, https://doi.org/10.1177/16878132231189070
[14] Shiyuan E, Wang Y, Xie B & Lu F, "A reliability-based robust design optimization method for rolling bearing fatigue under cyclic load spectrum", *Mathematics*, Vol. 15, No. 9, (2023), Article 16878132231189070, https://doi.org/10.3390/math11132843
[15] Lai X, Huang J, Zhang Y, Wang C & Zhang X, "A general methodology for reliability-based robust design optimization of computation-intensive engineering problems", *Journal of Computational Design and Engineering*, Vol. 9, No. 5, (2022), pp. 2151-2169, https://doi.org/10.1093/jcde/qwac096
[16] Wang Y, E S, Yang K, Xie B & Lu F, "Reliability-based robust design optimization with fourth-moment method for ball bearing wear", *Lubricants*, Vol. 12, No. 8, (2024), Article 293, https://doi.org/10.3390/lubricants12080293
[17] Tu J, Choi KK & Park YH, "A new study on reliability-based design optimization", *Journal of Mechanical Design*, Vol. 121, No. 4, (1999), pp. 557-564, https://doi.org/10.1115/1.2829499

[18] Du X & Chen W, "Sequential optimization and reliability assessment method for efficient probabilistic design", *Journal of Mechanical Design*, Vol. 126, No. 2, (2004), pp. 225-233, https://doi.org/10.1115/1.1649968
[19] Jiang Z, Chen X & Song Y, "Time-dependent reliability-based design optimization of main shaft bearings", *Reliability Engineering & System Safety*, Vol. 243, (2024), Article 109817, https://doi.org/10.1016/j.ress.2023.109817
[20] Karar N, Felkaoui A & Djeddou F, "Reliability-based robust design optimization based on sensitivity and elasticity factors analysis", *Journal of Materials and Engineering Structures*, Vol. 7, No. 1, (2020), pp. 97-111, https://revue.ummto.dz/index.php/JMES/article/view/2158, last visit: 16.07.2026.
[21] Perdana M A P et al., "Crashworthiness enhancement: The optimization of vehicle crash box performance by utilizing bionic-*Albuca spiralis* thin-walled structure", *Evergreen*, Vol. 10, No. 3, (2023), pp. 1961-1967, https://doi.org/10.5109/7151754
[22] Cai Z, Li W, Liu X & Zhang Y, "Mechanical properties of the novel spider-web bionic structure under axial impact loading", *Applied Physics A*, Vol. 130, No. 57, (2024), Article 57, https://doi.org/10.1007/s00339-023-07248-y
[23] He L, Li Y, Torrent D, Zhuang X, Rabczuk T & Jin Y, "Machine learning-assisted intelligent design of meta-structures: A review", *Microstructures*, Vol. 3, (2023), Article 2023037, https://doi.org/10.20517/microstructures.2023.29
[24] Deaton JD & Grandhi RV, "A survey of structural and multidisciplinary continuum topology optimization: Post 2000", *Structural and Multidisciplinary Optimization*, Vol. 49, No. 1, (2014), pp. 1-38, https://doi.org/10.1007/s00158-013-0956-z
[25] Dassault Systèmes, *Abaqus/Explicit User's Guide*, Dassault Systèmes Simulia Corp., Providence, RI, USA, (2024).